Lattice location and ionic state of Tm ions implanted into CaF_2

Y. Kido, H. Nakano, and T. Harami
Department of Physics, Faculty of Science and Engineering, Ritsumeikan University, Kita-ku, Kyoto 603, Japan

K. Ishii
Department of Physics Engineering, Faculty of Engineering, Kyoto University, Sakyo-ku, Kyoto 606, Japan

S. Yamashita
Nihon Kessyou-kogaku Corporation, Tatebayashi, Gunma 374, Japan

K. Shimomura and S. Matsuki
Research Centre for Nuclear Physics, Osaka University, Mihogaoka, Ibaragi, Osaka-fu 567, Japan
(Received 1 October 1990; revised manuscript received 4 October 1991)

Tm^+ ions with 100-keV energy were implanted into (111)-cut CaF_2 single crystals at 90 K and room temperature (RT). Ion backscattering using 1.5-MeV He^+ beams has revealed drastic inward diffusion of the implanted Tm ions and of the induced defects. Ion-channeling analysis has shown that the majority of the implanted Tm ions occupies a substitutional site replacing Ca^{2+}. The ionic state of the implanted Tm ions is determined by optical absorption and ion-beam-induced luminescence (IBIL) analyses and the divalent fraction is estimated to be 60–90 %. The IBIL spectra are compared with those resulting from ultraviolet-light excitation. No significant difference is seen between the characteristics of the Tm ions implanted at 90 K and RT.

I. INTRODUCTION

Ion implantation has recently been utilized to investigate the characteristics of unstable nuclei far off the β-stability line.[1,2] In this case short-lived isotopes produced by spallation reactions with high-energy particles from a high-energy accelerator are implanted into solids with an isotope separator. The magnetic circular dichroism of rare-earth atoms in alkaline-earth fluoride hosts is so large that the electron-spin polarization can be significantly enhanced by pumping with circularly polarized laser light in the visible region. The electron polarization is then transferred to the nuclei mainly through the hyperfine interaction. Unstable $^{170}Tm^{2+}$ ions in alkaline-earth fluorides provide a typical and interesting example to achieve appreciable nuclear polarization, thereby determining the nuclear magnetic moment by the detection of the asymmetry of the emitted β rays.[3]

Unfortunately, not enough is known about the characteristics of the implanted ions and the induced lattice damage for alkaline-earth fluoride crystals.[4–6] The aim of the present work is to determine the lattice position together with the ionic state of Tm ions implanted into CaF_2 single crystals. Naturally, thulium exists as a trivalent ion in CaF_2. In this case a F^- ion exists in one of the six nearest-neighbor (dodecahedral) interstitial sites at a distance of half the lattice constant from the substitutional Tm^{3+} ion.[7,8] However, it has been reported that a trivalent-to-divalent conversion can easily occur by x- or γ-ray irradiation or by annealing in a Ca vapor.[9,10] This suggests that preferential F-vacancy production is essential to promote the trivalent-to-divalent conversion. Thus we expect that a considerable fraction of divalent Tm should be obtained directly by Tm^+ implantation into CaF_2.

In the present experiment, stable $^{169}Tm^+$ ions with 100 keV energy were implanted into (111)-cut CaF_2 single crystals at low (90 K) and room temperatures (RT). The lattice-location measurement together with depth profiling of the implanted Tm and the induced defects was made by ion backscattering with 1.5-MeV He^+ ions. Optical-absorption and ion-beam-induced luminescence measurements were performed to determine the ionic state of the implanted Tm ions.

II. EXPERIMENT

The mirror-finished (111)-cut CaF_2 crystals were etched chemically in a solution of HCl (10 cm^3: 35 wt. %) and H_2O (50 cm^3) for 2–3 min. Then they were rinsed in acetone with an ultrasonic cleaner. After this treatment we obtained a χ_{min} value of 0.03–0.04 by ion-channeling analysis, which certifies the complete elimination of surface-disordered layers. The size and purity of CaF_2 are $1.0\times1.0\times0.09$ cm^3 and 99.99 at. %, respectively.

The 100-keV Tm^+ implantation into CaF_2 was performed with the Cockcroft accelerator of Toyota R&D Laboratory. The CaF_2 samples were mounted on a rotatable holder, which can be cooled down to liquid-nitrogen temperature (77 K). In order to avoid the channeling incidence, the surface normal of the sample was tilted about 8° from the incident-beam direction. The accelerated Tm^+ ions were scanned vertically and horizontally with a couple of electrostatic deflectors to realize

uniform irradiation and to suppress electrical charging on the sample surface. The Tm^+-beam flux was set at 0.5–1 $\mu A/cm^2$, and a temperature rise of 20 °C at most was observed immediately after Tm^+ irradiation. We used a Chromel-Alumel thermocouple, which was inserted between the sample and the sample holder made of copper. The sample-temperature measurement could not be made during Tm^+ irradiation because of ion-irradiation-induced electric noise upon the thermocouple signal. The present implantation temperatures of 300 K (RT) and 90 K are the average and approximate ones measured immediately after the Tm^+ irradiation. The operating pressure in the irradiation chamber was maintained at less than 8×10^{-7} Torr using a turbomolecular pump combined with a liquid-nitrogen trap. Thus the amount of contamination such as carbon buildup on the Tm^+-irradiated surface was kept within a small level and the irradiated samples were found to have almost the same transparency compared with nonirradiated ones.

The lattice location of the implanted Tm ions together with the depth profiles of the implanted Tm and produced defects was measured by 1.5-MeV He^+ backscattering using the ion-channelling effect. For precise spectrum analysis, we best fitted the computer-simulated backscattering spectrum to the corresponding observed one.

In order to determine the absolute quantity of divalent Tm in CaF_2, we prepared trivalent and divalent Tm-doped CaF_2 samples. First, a standard sample containing trivalent Tm ions only was synthesized by the Bridgman method with CaF_2 seed crystals. The trivalent-to-divalent conversion was accomplished by annealing at 800 °C for 10 h in a Ca vapor with 0.45 Torr pressure. According to the report of Kiss and Yocom,[9] this annealing condition is sufficient to complete the trivalent-to-divalent conversion. In fact, the color changed from transparency to green after the heat treatment. We can derive the divalent Tm concentration in CaF_2 from the optical-absorption spectrum measured at RT and liquid-nitrogen temperature (LNT) in a wide wavelength range from 200 to 1500 nm. The optical density (OD) which is defined by $\log_{10}(I_0/I)(I/I_0$, transmittance), is proportional to the Tm^{2+} concentration C (at. %) and to the sample thickness t (cm):

$$\log_{10}(I_0/I)=aCt \ , \tag{1}$$

where a is the proportionality constant.

Mitsunaga[11] recommended to use the optical density at a wavelength of 590 nm measured at RT and an a value of 2.9×10^2 (at. % cm)$^{-1}$ for determining the absolute quantity of the divalent Tm in CaF_2. Thus we obtain a divalent concentration of 0.075 at. % for the present divalent standard sample.

We expect that ion-beam-induced luminescence is very sensitive to the ionic state of the implanted Tm ions localizing near a surface region. In the present experiment, we employed 200-keV Ar^+ beams provided by the 300-kV Disktron accelerator of Kyoto University and measured the luminescence spectra with a Czerny-Turner monochromator in the wavelength range from 400 to 650 nm. A pair of quartz lenses was used to focus a segment of the light beam onto the entrance slit of the monochromator with unit magnification. The monochromator was driven in steps at discrete wavelength intervals of 1 nm, and the photon counting was normalized by the integrated Ar^+-beam current.

III. LATTICE LOCATION

Figure 1 shows the random and [111]-aligned backscattering spectra from the CaF_2 crystals before and after the 100-keV Tm^+ implantation (1×10^{16} Tm^+/cm^2 at 90 K). The spectra drawn with points and solid curves are the observed and corresponding best-fitted ones, respectively. Here the calculation of the dechanneling fractions was made according to the method proposed by Feldman and Rodgers.[12] The depth profiles of the implanted Tm and induced defects were assumed to be asymmetric Gaussian shapes.[13]

The induced defect profile was determined from the best-fitting condition for the above aligned spectrum and is shown in Fig. 2. For comparison, this figure includes the defect profiles for the Tm^+ implantation with doses of 1×10^{15} and 1×10^{16} Tm^+/cm^2 at RT together with the calculated defect profile (histogram) from the Monte Carlo simulation code TRIM,[14] which is based on the binary-collision approximation. The present result reveals a much deeper defect concentration profile than expected from the theoretical estimate. The defect profile for the sample implanted at 90 K is slightly larger than that at RT, as shown in Fig. 2. The present experiment shows an inward diffusion of the induced defects with increasing Tm^+ dose. For low Tm^+ dose, the defect profile approaches the calculated one.

The Tm depth profile derived from the best fitting of the random spectrum is depicted with a solid curve in Fig. 3. The implanted Tm ions diffuse remarkably toward the inside, as it clearly seen from the comparison with the Tm profile calculated from the TRIM code (histogram). The inward diffusion is enhanced with increasing

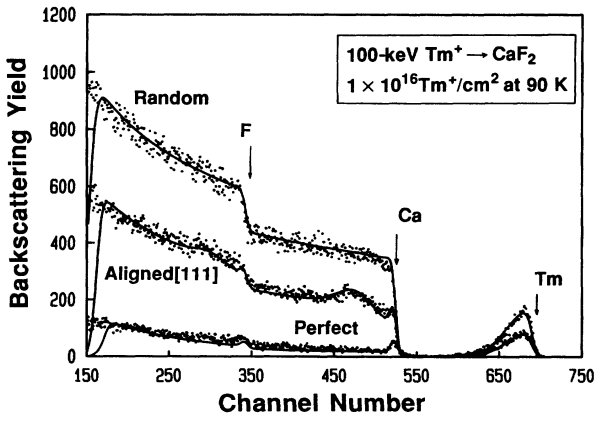

FIG. 1. Random and [111]-aligned backscattering spectra from CaF_2 crystals before and after 100-keV Tm^+ implantation at 90 K with a dose of 1×10^{16} Tm^+/cm^2. The spectra depicted with points and solid curves correspond to the observed and best-fitted ones, respectively.

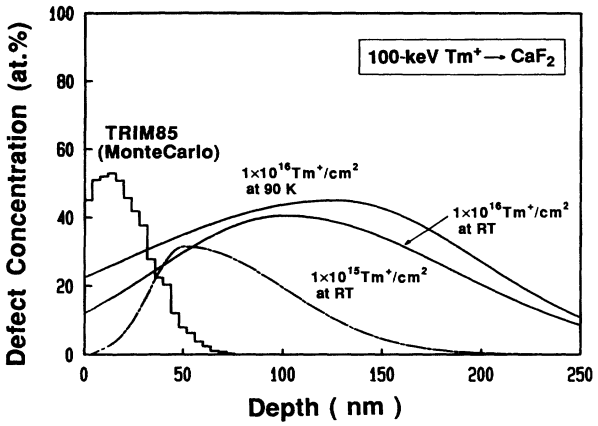

FIG. 2. Dose and temperature dependence of the induced defect concentrations for 100-keV Tm^+-implanted CaF_2 crystals. The histogram denotes the defect profile calculated from the Monte Carlo simulation code TRIM.

Tm^+ dose for both the 90-K and RT implantations. Such behavior is quite similar to that of the induced defects. Townsend[6] pointed out that pronounced electronic sputtering of halogens occurs for energetic ion-bombarded alkali halides. However, the amount of the self-sputtered Tm is estimated to be 2×10^{14} Tm/cm^2 from the above Tm depth profile and thus negligibly small compared with the amount of the implanted Tm (1×10^{16} Tm^+/cm^2).

Here we consider the heating-up effect of the ion irradiation upon the anomalous inward diffusion. As mentioned in Sec. II, the temperature rise of about 20 °C was observed with the thermocouple immediately after the Tm^+ irradiation. Such a macroscopic temperature rise does not have a significant effect on the above anomalous diffusion. We can roughly estimate the local and instantaneous temperature rise in the collision cascade region right under the beam spot. According to the method proposed by Nakata,[15] we obtain a local temperature rise of at most 10 °C under the present implantation condition. Thus the anomalous inward diffusion of the implanted Tm and of the induced defects is not explained adequately by the macroscopic and/or local temperature rise during Tm^+ irradiation.

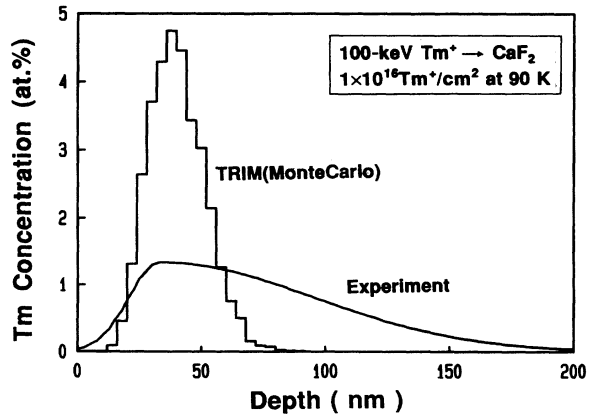

FIG. 3. Depth profile of the implanted Tm ions derived from the best fitting of the observed random spectrum. The CaF_2 sample was implanted with 100-keV Tm^+ at 90 K with a dose of 1×10^{16} Tm^+/cm^2. The histogram is the Tm depth profile calculated from TRIM.

As another possibility to explain the anomalous inward diffusion we must consider the electrical charging up of the irradiated sample surface. If the top surface irradiated with Tm^+ is positively charged owing to the secondary-electron emission, the Tm and displaced Ca ions diffuse inward by the repulsive electric force. In order to suppress the charging-up effect, we scanned the Tm^+ beam in a wide range of 2.5×2.5 cm^2 around the sample with the size of 1.0×1.0 cm^2 at the scanning frequency of 1 kHz. We have not experienced so far such anomalous diffusion for the metal ion-implanted insulator materials such as sapphire and zirconia crystals under the same implantation condition. Thus the anomalous inward diffusion upon the charging-up effect is expected to be small.

From the above discussion, we should consider other physical or chemical effects of ion irradiation to explain the present pronounced inward diffusions of defects and implanted Tm ions. Here we note that the Monte Carlo simulation neglects the electronic process for ion-beam-induced defect formation and for migration of implanted ions. Townsend[6] pointed out that energetic secondary electrons or exciton motion may play an important role in deep defect migration. Such electronic processes may lead to pronounced inward diffusions of defects and implanted ions, in particular for alkali and alkaline-earth fluorides.

As shown in Fig. 1, the [111]-aligned backscattering yield from Tm is much smaller than the random yield. Such a reduction is ascribed to the shadowing effect of the crystal rows, and the subtraction of the aligned yield from the random yield leads to the number of Tm ions lying in the [111] row. In fact, the shadow cone radius is very small and calculated to be less than 0.01 nm in the case of 1.5-MeV He^+ ion channeling along the CaF_2 [111] axis. We also measured the [110]-aligned backscattering spectra and obtained almost the same reduction rates of [110]-aligned to random yields from Tm as those of [111]-aligned to random ones. Here we should note that the most possibly occupied interstitial site is the dodecahedral one, which is shadowed for [111]-aligned beams, but not for [110]-aligned ones. It is therefore suggested, also from the charge balance, that the positively charged implanted Tm ions occupy the substitutional lattice position, replacing Ca^{2+}. Figure 4 shows the substitutional Tm fractions (circles) determined from channeling spectra together with the maximum defect concentration (squares), as a function of Tm^+ dose. The solid and half-solid symbols denote the implantation at 90 K and the implantation at RT followed by annealing at 500 °C for 1 h, respectively. With increase in Tm^+ dose, the number of induced defects becomes large, while the substitutional fraction seemingly decreases. The substitutional Tm fraction F_s and the maximum defect concentration C_{max} have a complementary relation in the form $F_s + C_{max} \cong 100$ at. %. This relation suggests that the seemingly small substitutional fractions for high Tm^+

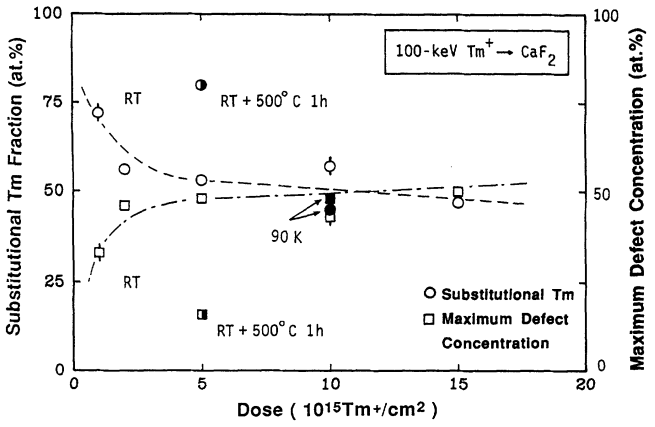

FIG. 4. Dose dependence of the substitutional Tm fractions (circles) together with the maximum defect concentration (squares) for RT implantation. The solid and half-solid symbols denote the 90-K and RT implantations followed by annealing at 500 °C for 1 h, respectively.

dose are ascribed to the partially induced lattice disorder and that the majority of the implanted Tm ions occupies the substitutional site. As will be seen later, this is confirmed by optical-absorption and ion-beam-induced luminescence analyses.

Moore and Wright[7] and Catlow, Chadwick, and Corish[16] determined the local structures surrounding the dopant ions for Er- and La-doped CaF_2 using the techniques of neutron diffraction and extended x-ray-absorption fine structure (EXAFS). They reported that the trivalent dopant ion occupies a lattice cation site with the extra charge compensated for by an interstitial F^- in a neighboring, interstitial cube center site in low dopant concentration (<0.5 mol %), while for higher concentrations (>10 mol %) aggregation of the simple pairs of substitutional dopant and fluoride interstitial occurs. The Tm concentration in the present Tm^+-implanted samples is at a not so high level ($<$ a few mol %), and thus the high substitutional fraction of implanted Tm is consistent with the above local structures. Aside from the detailed local structure, in the next subsection we determine the ionic state of substitutional Tm and the Tm^{2+} fraction by optical-absorption and ion-beam-induced luminescence measurements.

IV. IONIC STATE

As mentioned previously, the Tm ions doped into CaF_2 using Bridgman method exist as trivalent ions under the thermal equilibrium condition, but the trivalent-to-divalent conversion can occur by subsequent treatments such as x- or γ-ray irradiation and annealing at high temperatures in a Ca vapor. Our interest is centered on how much divalent fraction is obtained by direct Tm^+ implantation into CaF_2 at RT and LNT. In order to determine the ionic state of the implanted Tm ions, we first measured the electron-spin-resonance (ESR) spectra at LNT, but observed only the signals originating from the induced defects for Tm^+-implanted CaF_2. Then we tried the optical-absorption analysis and the ion-beam-induced luminescence measurements.

A. Optical absorption

Figure 5 shows schematic energy-level diagrams from the divalent and trivalent Tm ions in CaF_2.[9,17] The $^2F_{7/2}$ and $^3H_6$ states correspond to the ground states of Tm^{2+} and Tm^{3+}, respectively, and the cubic field of the CaF_2 crystal further splits each electronic level of the Tm ions into several sublevels. The electrons excited to the absorption bands make a very fast transition to the $^2F_{5/2}$ state, which is a metastable state with a lifetime of 5 ms.[17]

As described in Sec. II, absorption bands were observed for the Tm^{2+} standard sample, while we observed no significant absorption lines for the Tm^{3+} standard sample in the visible region. Figures 6(a) and 6(b) show the optical densities measured at LNT for the Tm^2 standard sample (0.075 at. %) and for the Tm^+-implanted CaF_2 crystal, respectively, in the wavelength range from 200 to 700 nm. The latter was prepared by implanting 100-keV Tm^+ ions into the front and back surfaces of the CaF_2 crystal equivalently with a total dose of 2×10^{16} Tm^+/cm^2 at RT. The absorption band structure for the Tm^+-implanted CaF_2 is similar to that for the Tm^{2+} standard sample except for the weak peak intensities and considerable peak broadening. From the intensity ratio of the 590-nm peak, we derived a Tm^{2+} fraction of 72% for the Tm^+-implanted CaF_2 sample. The ratio of the standard to the Tm^+-implanted spectral areas [indicated with shaded areas in Figs. 6(a) and 6(b)] gives a Tm^{2+} fraction of about 90%. Such analyses were made for three different Tm^+-implanted CaF_2 crystals, and the resultant Tm^{2+} fractions range from 60% to 90%. No significant difference was obtained between the Tm^{2+} fractions for the Tm ions implanted at RT and 90 K.

The accuracy of the present optical-absorption analysis is not as satisfactory because of uncertainties in the deconvoltion and background subtraction procedure. In addition, the shape of the absorption peak for the Tm^+-implanted CaF_2 is different from that of the Tm^{2+} stan-

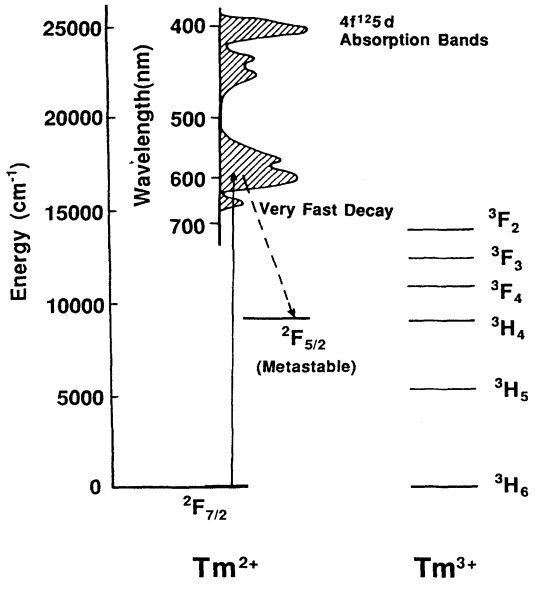

FIG. 5. Energy-level diagrams for Tm^{2+} and Tm^{3+} in CaF_2.

dard sample. This is probably due to damage effects such as crystal lattice distortion induced by Tm^+ implantation. However, it is certain that a considerable Tm^{2+} fraction can be obtained directly by Tm^+ implantation into CaF_2 even at LNT. The present estimate is supported by the result of ion-beam-induced luminescence measurements, as will be described in the following subsection.

B. Ion-beam-induced luminescence

The optical density is proportional to the total amount of dopant atoms, and therefore it is extremely weak for the ion-implanted samples except for samples prepared by high-dose implantation. On the other hand, ion-beam-induced luminescence should have an excellent sensitivity to the implanted dopants localized near the surface region because of the high probability of electronic excitation by fast heavy ions. As illustrated in Fig. 5, the electrons excited to the absorption bands decay very fast into the metastable $^2F_{5/2}$ state, whereupon the visible photoemission occurs. Recently, Aono, Iwaki, and Namba[18] observed the luminescence from Eu^+-implanted CaF_2 during the implantation and also detected the same luminescence spectrum by subsequent Ar^+ irradiation. They regarded the several broad lines observed as the emission from Eu^{2+} or Eu^{3+} in CaF_2.

The solid curves in Figs. 7(a) and 7(b) show the Ar^+-induced luminescence spectra from the Tm^{2+} and Tm^{3+} standard samples, respectively. The spectrum from a nondoped CaF_2 crystal is depicted with points. A number of narrow peaks seen for both standard samples originating from the interaction of the argon beam with the

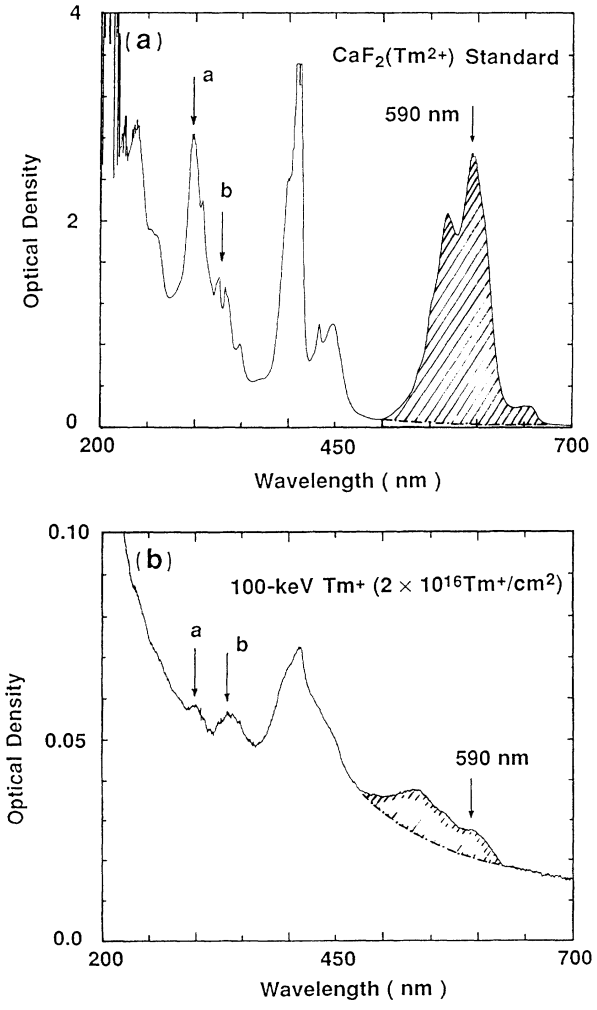

FIG. 6. (a) Observed optical-absorption spectrum from the divalent Tm standard sample. (b) Observed optical-absorption spectrum from the Tm^+-implanted CaF_2 sample with a total dose of 2×10^{16} Tm^+/cm^2.

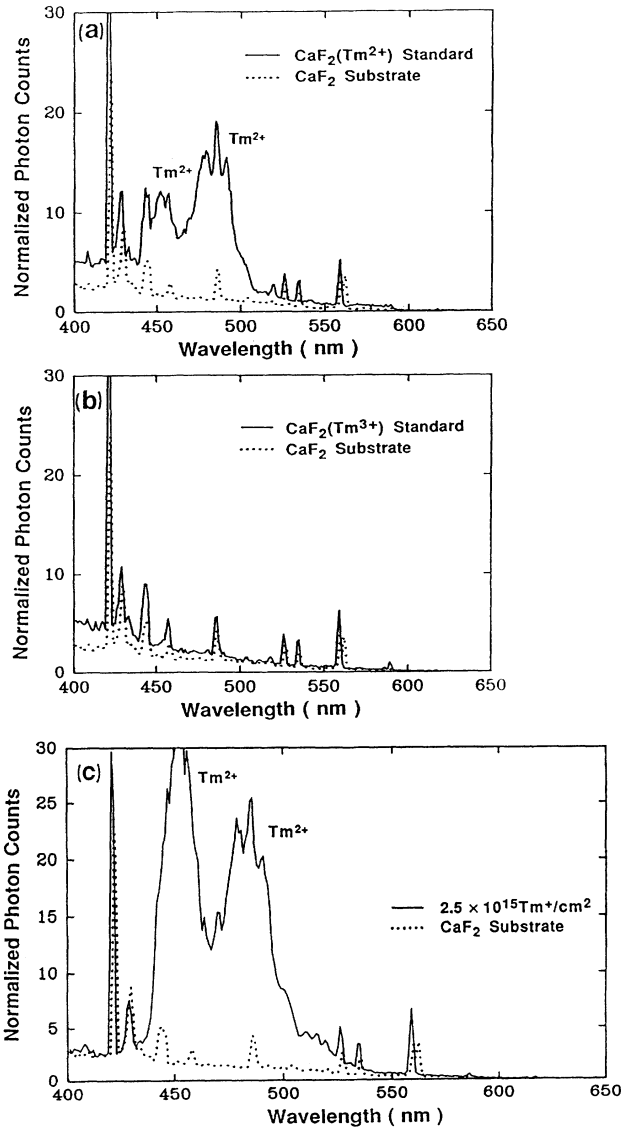

FIG. 7. (a) 200-keV Ar^+-induced luminescence spectra from the divalent Tm standard sample (solid curve) and from the nondoped CaF_2 crystal (points). (b) 200-keV Ar^+-induced luminescence spectra from the trivalent Tm standard sample (solid curve) and from the nondoped CaF_2 crystal (points). (c) 200-keV Ar^+-induced luminescence spectra from the CaF_2 sample before (points) and after (solid curve) 100-keV Tm^+ implantation at RT with a dose of 2.5×10^{15} Tm^+cm^2.

CaF_2 crystal. Two broad peaks around the wavelengths 455 and 485 nm were observed for the Tm^{2+} standard sample, whereas no significant peak was observed for the Tm^{3+} standard sample. Figure 7(c) shows the observed luminescence spectrum from the Tm^+-implanted CaF_2 sample with a dose of 2.5×10^{15} Tm^+/cm^2. In spite of the small amount of implanted Tm ions, we observed two strong broad peaks with wavelengths coinciding with those observed for the Tm^{2+} standard sample. The intensity ratio of these two peaks in Fig. 7(c) is reversed in contrast with that for the Tm^{2+} standard sample. This is probably related to a delicate change of atomic configurations such as crystal-lattice distortion induced by the Tm^+ implantation. The ratio of the spectral area around 455 and 485 nm for Tm^+ implanted to that for the Tm^{2+} standard sample is about 2.5. Now we roughly estimate the Tm^{2+} fraction assuming that the excitation probability for Tm^{2+} is proportional to the electronic stopping power of Tm implanted into CaF_2. The electronic stopping power depends strongly upon the Ar^+ energy $E(x)$ at depth x,

$$E(x)=E_0-\int_0^x S(E(x))dx \ , \tag{2}$$

where E_0 is the incident Ar^+ energy and $S(E)$ is the total stopping power of CaF_2 (Tm) for Ar ions. The stopping power $S(E)$ is expressed by

$$S(E)=[1-C_{\mathrm{Tm}}(x)]S_e^{\mathrm{Ca}}(E)/3+2[1-C_{\mathrm{Tm}}(x)]S_e^{\mathrm{F}}(E)/3 +C_{\mathrm{Tm}}(x)S_e^{\mathrm{Tm}}(E)+S_n(E) \ . \tag{3}$$

Here the first three terms correspond to the contributions from the electronic stopping powers of Ca, F, and Tm and $S_n(E)$ is the nuclear stopping power originating from elastic scattering. The Tm concentration $C_{\mathrm{Tm}}(x)$ at depth x is determined by ion backscattering in the form of an asymmetric Gaussian shape. For the Tm^{2+} standard sample, $C_{\mathrm{Tm}}(x)=7.5\times10^{-4}$. The integrated photon intensity around 455 and 485 nm is given by

$$I=k\int_0^{x_p} C_{\mathrm{Tm}}(x)S_e^{\mathrm{Tm}}(E(x))dx \ , \tag{4}$$

where k is an arbitrary constant and x_p is the projected range of 200-keV Ar^+ ions in CaF_2. To perform the numerical calculation, we employed the semiempirical electronic-stopping-power formula reported by Ziegler, Biersack, and Littmark[19] and the nuclear-stopping-power formula proposed by Wilson, Haggmark, and Biersack.[20] The present analysis gives the Tm^{2+} fraction of about 70 at. %, which is consistent with that derived from the optical-absorption measurement.

It is interesting to compare the ion-beam-induced luminescence spectra with the emission spectrum obtained by optical pumping. Figure 8(a) shows the 300-nm photon-induced emission spectrum from the Tm^{2+} standard sample. The several peaks originate from transitions from the absorption bands to the $^2F_{5/2}$ state (see Fig. 5). The excitation light was introduced from a Xe lamp through a monochromator, but the wavelength width is considerably wide, as seen from this emission spectrum. Figure 8(b) shows the excitation spectra with 350- and 395-nm photon detection, which clearly indicate that the 350- and 395-nm emission lines originate from 265- and 300-nm photon absorption, respectively. Thus the 395-nm emission corresponds to the 300-nm absorption band, [*a*, indicated in Fig. 6(a)], but the origin of the 350-nm emission is not clear. Opposed to our expectation, the observed primary two peaks in the Ar^+-induced luminescence spectra do not correspond well to any peaks in the photon-induced emission spectrum. This is possibly due to the fact that such heavy-ion penetration destroys the original atomic and electronic configurations and/or accompanies complicated excitation processes.

Finally, we discuss qualitatively the mechanism to achieve the high Tm^{2+} fraction by direct Tm^+ implantation into CaF_2. In the case of annealing the Tm^{3+} standard sample in a Ca vapor, preferential production of F vacancies occurs as a result of the production of excess of Ca^{2+}. The F^- ions located in the vicinity of Tm^{3+} ions move into these vacancies, and thus the trivalent-to-divalent conversion is realized. The Tm^+ implantation

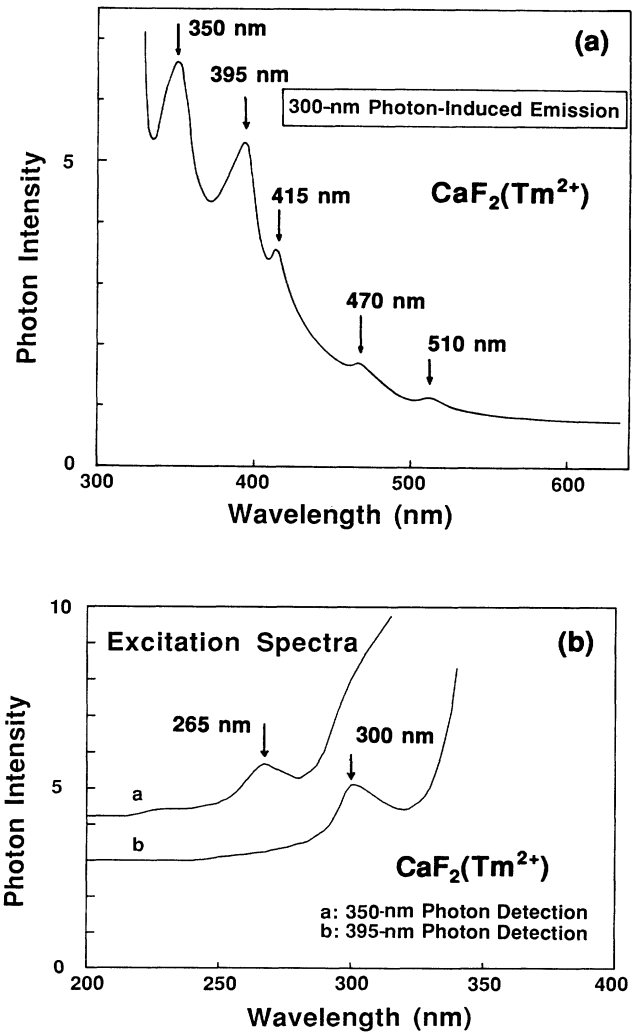

FIG. 8. (a) Photon emission from the Tm^{2+} standard sample subsequent to the absorption of the ultraviolet light with the wavelength of 300 nm. (b) Excitation spectra with 350- and 395-nm photon detection for the Tm^{2+} standard sample.

also introduces a number of F vacancies preferentially because of the small displacement energy and as described in Sec. III, a drastic vacancy migration occurs. Therefore, even if the substitutional occupation by Tm^{3+} is initially predominant, the interstitial F^- ions connected with the Tm^{3+} ions can move into the F vacancies and then the substitutional Tm^{2+} state is stabilized from the charge balance.

V. SUMMARY

We have measured the lattice location and ionic state of Tm ions implanted into CaF_2 single crystals at RT and 90 K. The ion backscattering using 1.5-MeV He^+ beams has shown that the majority of the implanted Tm ions occupies the substitutional Ca lattice position. The present experiment has also revealed a drastic inward diffusion of the implanted Tm ions and of the induced defects. The effects of the macroscopic and/or local temperature rise and of the surface charging up are ruled out. It is closely related to the preferential production and subsequent migration of F vacancies as well as of vacancy complexes, which are characteristic phenomena during ion irradiation of alkali and alkaline-earth fluorides. In the above phenomena, energetic secondary electrons or exciton motion possibly play an important role.

The ionic state of the Tm ions implanted into CaF_2 was determined from the optical-absorption and ion-beam-induced luminescence spectra. The Tm^{2+} fraction of the implanted Tm was estimated to be 60–90%. We can qualitatively understand the mechanism to attain such a high Tm^{2+} fraction by direct Tm^+ implantation into CaF_2. First, energetic Tm ions penetrating CaF_2 produce preferentially a number of F vacancies because of the small displacement energy. Then a drastic vacancy migration occurs during the implantation. Thus the F^- interstitials which can stabilize the substitutional Tm^{3+} ions tend to move into the F vacancies which migrate in the vicinity of them. Such pronounced mobilities of the vacancies and Tm ions are essential to realize high Tm^{2+} fractions.

The ion-beam-induced luminescence is much more sensitive to the ionic state of the Tm ions localized near the surface region than the optical absorption. The 200-keV Ar^+-induced luminescence gives primary two peaks originating from Tm^{2+} in CaF_2, but their wavelengths do not coincide with the transitions from the absorption bands to the metastable $^2F_{5/2}$ state. This inconsistency suggests that such heavy-ion penetration destroys the original atomic and electronic configurations and accompanies multiple excitation and ionization processes. The present situation may be improved by using MeV light ions such as H^+ and He^+, although the luminescence intensity is expected to decrease to a certain extent.

ACKNOWLEDGMENTS

The authors would like to thank Dr. J. Nakata of NTT LSI Laboratory and Dr. M. Ohkubo of Toyota R&D Laboratory for valuable discussion concerning the temperature rise during ion irradiation. Thanks are also due to Dr. S. Kakigi for cooperation in carrying out the optical-absorption analysis. They gratefully acknowledge the technical support of the staff members of Toyota R&D Laboratory and Plasma Science Laboratory of Kyoto University. This study was supported in part by a Grant-in-Aid for Scientific Research from the Ministry of Education, Science and Culture, Japan.

[1]E. W. Otten, Hyperfine Interact. **34**, 3 (1987).
[2]E. Arnold, J. Bonn, R. Gegenwart, W. Neu, R. Neugart, E. W. Otten, G. Ulm, and K. Wendt, Phys. Lett. **197**, 311 (1987).
[3]K. Shimomura, S. Uemura, T. Kohmoto, Y. Fukuda, S. Ito, K. Okano, T. Muramoto, T. Hashi, and S. Matsuki, Phys. Rev. C **42**, R487 (1990).
[4]U. Bangert, K. Thiel, K. Ahmed, and P. D. Townsend, Radiat. Eff. **64**, 143 (1982).
[5]J. Kowalski, G. Marest, A. Perez, B. D. Sawicka, J. A. Sawicki, J. Stanek, and T. Tyliszczak, Nucl. Instrum. Methods **209/210**, 1145 (1983).
[6]P. D. Townsend, Rep. Prog. Phys. **50**, 501 (1987).
[7]D. S. Moore and J. C. Wright, J. Chem. Phys. **74**, 1626 (1981).
[8]C. R. A. Catlow, L. M. Moroney, A. V. Chadwick, and G. N. Greaves, Radiat. Eff. **75**, 159 (1983).
[9]Z. J. Kiss and P. N. Yocom, J. Chem. Phys. **41**, 1511 (1964).
[10]W. B. Grant, L. F. Mollenauer, and C. D. Jefferies, Phys. Rev. B **4**, 1428 (1971).
[11]M. Mitsunaga, Ph.D. thesis, University of California, Berkeley, 1983.
[12]L. C. Feldman and J. W. Rodgers, J. App. Phys. **41**, 3776 (1970).
[13]Y. Kido and J. Kawamoto, J. Appl. Phys. **61**, 956 (1987).
[14]J. P. Biersack and L. G. Haggmark, Nucl. Instrum. Methods **174**, 257 (1980).
[15]J. Nakata, Phys. Rev. B **43**, 14 643 (1991).
[16]C. R. A. Catlow, A. V. Chadwick, and J. Corish, Radiat. Eff. **75**, 61 (1983).
[17]E. S. Sabisky and C. H. Anderson, IEEE J. Quantum Electron. **QE-3**, 287 (1967).
[18]K. Aono, M. Iwaki, and S. Namba, Nucl. Instrum. Methods B **32**, 231 (1988).
[19]J. F. Ziegler, J. P. Biersack, and U. Littmark, *The Stopping and Range of Ions in Solids* (Pergamon, New York, 1985).
[20]W. D. Wilson, L. G. Haggmark, and J. P. Biersack, Phys. Rev. B **15**, 2458 (1977).